

Precision flatness measurement based on orbital angular momentum

Feifei Han(韩菲菲), Zhiwan Wang(王志琬), Le Wang(王乐), and Shengmei Zhao(赵生妹)
Citation: Chin. Phys. B, 2025, 34 (**5**): 054204. DOI: 10.1088/1674-1056/adbd14
http://cpb.iphy.ac.cn; http://iopscience.iop.org/cpb

What follows is a list of articles you may be interested in

Controlled propagation and particle manipulation of off-axis-rotating elliptical Gaussian beams in strong nonlocal media

Rong-Quan Chen(陈荣泉), Rui-Lin Xiao(肖瑞林), Wei Wang(王伟), Xi-Xi Chu(储茜茜), Yu-Qing Song(宋雨晴), Xu-Dong Hu(胡旭东), and Ming Chen(陈明)
Chin. Phys. B, 2025, 34 (**3**): 034205. DOI: 10.1088/1674-1056/ada9dd

Interface state-based bound states in continuum and below-continuum-resonance modes with high-*Q* factors in the rotational periodic system

Jialing Yang(杨嘉玲), Aoqian Shi(史奥芊), Yuchen Peng(彭宇宸), Peng Peng(彭鹏), and Jianjun Liu(刘建军)
Chin. Phys. B, 2024, 33 (**8**): 084206. DOI: 10.1088/1674-1056/ad4630

Optimization of extreme ultraviolet vortex beam based on high harmonic generation

Bo Xiao(肖礴), Yi-Wen Zhao(赵逸文), Fang-Jing Cheng(程方晶), Ge-Wen Wang(王革文), Wei Jiang(姜威), Yi-Chen Wang(王一琛), Jie Hu(胡杰), Hong-Jing Liang(梁红静), and Ri Ma(马日)
Chin. Phys. B, 2024, 33 (**5**): 054209. DOI: 10.1088/1674-1056/ad2bf0

Effectively modulating spatial vortex four-wave mixing in a diamond atomic system

Nuo Ba(巴诺), Ming-Qi Jiang(姜明奇), Jin-You Fei(费金友), Dan Wang(王丹), Hai-Lin Jiang(蒋海林), Lei Wang(王磊), and Hai-Hua Wang(王海华)
Chin. Phys. B, 2024, 33 (**4**): 044202. DOI: 10.1088/1674-1056/ad0771

Generation of orbital angular momentum hologram using a modified U-net

Zhi-Gang Zheng(郑志刚), Fei-Fei Han(韩菲菲), Le Wang(王乐), and Sheng-Mei Zhao(赵生妹)
Chin. Phys. B, 2024, 33 (**3**): 034207. DOI: 10.1088/1674-1056/ad12aa

---

Precision flatness measurement based on orbital angular momentum

Feifei Han(韩菲菲)[1], Zhiwan Wang(王志琬)[1], Le Wang(王乐)[1], and Shengmei Zhao(赵生妹)[1,2,3,†]

[1] *Institute of Signal Processing and Transmission, Nanjing University of Posts and Telecommunications, Nanjing* 210003, *China*
[2] *Key Laboratory of Broadband Wireless Communication and Sensor Network Technology, Ministry of Education, Nanjing* 210003, *China*
[3] *National Laboratory of Solid State Microstructures, Nanjing University, Nanjing* 210093, *China*

(Received 20 November 2024; revised manuscript received 27 February 2025; accepted manuscript online 6 March 2025)

We propose a method to measure the flatness of an object with a petal-like pattern generated by the interference of the measured orbital angular momentum (OAM) beam and the reference OAM beam which carries the opposite OAM state. By calculating the difference between the petal rotation angle without/with the object, the thickness information of the object, and then the flatness information, can be evaluated. Furthermore, the direction of the object's flatness can be determined by the petal's clockwise/counterclockwise rotation. We theoretically analyze the relationship between the object's thickness and petal rotation angle, and verify the proposed method by experiment. The experimental results show that the proposed method is a high precision flatness measurement and can obtain the convex/concave property of the flatness. For the 1.02 mm glass sample, the mean deviation of the flatness is 1.357×10^{-8} and the variance is 0.242×10^{-16}. For the 0.50 mm glass sample, the mean deviation of the flatness is 1.931×10^{-8} and the variance is 2.405×10^{-16}. Two different topological charges are adopted for the 2.00 mm glass sample, and their flatness deviations are 0.239×10^{-8} ($\ell=1$) and 0.246×10^{-8} ($\ell=2$), where their variances are 0.799×10^{-18} ($\ell=1$) and 0.775×10^{-18} ($\ell=2$), respectively. It is shown that the flatness measured by the proposed method is the same for the same sample when different topological charges are used. All results indicate that the proposed method may provide a high flatness measurement, and will be a promising way to measure the flatness.

Keywords: orbital angular momentum, flatness measurement, interference, petal rotation angle

PACS: 42.50.Tx, 42.25.Hz, 43.20.Ye

DOI: 10.1088/1674-1056/adbd14 **CSTR:** 32038.14.CPB.adbd14

1. Introduction

The flatness is the difference between the unevenness and the absolute level. It indicates the maximum deviation from the plane of the surface, and the plane is generated by fitting the measured values at various positions. The precision measurement and evaluation of the geometry form error for high-end precision components is one of the most important tasks for metrologists.[1] It is often necessary to conduct a surface flatness inspection to evaluate the flatness quality of the target structure in practical applications, such as optical surfaces[2] and aero-engine rotor connection surfaces.[1]

Compared with other measurement methods, optical measurement has the advantages of high precision and no contact.[3] That is, the optical measurement can provide a highly precise measurement meanwhile it does not require contact with the measured object, so it can avoid the target object's deformation or damage, and it is especially safe and reliable for handling the sensitive or fragile materials. Among optical approaches, such as reflectometry,[4] ellipsometry,[5] confocal microscopy[6] and interferometry,[7] the optical interferometry method can measure thicknesses with direct traceability to a length standard. With the consideration of the demands by the semiconductor and display industries, the optical interferometry method is an optimal solution in terms of the measurement ranges used and levels of precision required.

Like amplitude, frequency and phase, orbital angular momentum (OAM) is a type of freedom of physical quantity carrying information. It has a spiral phase characterized by $\exp(\mathrm{i}l\theta)$, where θ is an azimuthal angle and ℓ is the topological charge (TC). In 1992, it was first experimentally demonstrated that each photon in the Laguerre–Gaussian (LG-OAM) beam had $\ell\hbar$ OAM.[8] The properties of the OAM state (the value of ℓ is ranged from the negative infinity to the positive infinity, the different ℓ OAM states are orthogonal to each other[9,10]) make the OAM's system capacity and frequency band utilization be greatly increased.[10–14] At present, OAM has been found in extensive applications in free optical communication,[15,16] optical communication,[17] wireless communication,[18] etc.

Also, the petal-like intensity distribution obtained by superimposing two OAM beams with opposite TC values has received wide attentions in high-precision measurement. For instance, Lavery *et al.* realized the detection of a rotating object by using a beam carrying OAM.[19] Guo *et al.* studied super-sensitive rotation measurements using an OAM atomic-optical hybrid interferometer.[20] Zhai *et al.* demonstrated the feasibility of the remote detection of a rotator based on the rotational Doppler effect.[21] Xiao *et al.* demonstrated

†Corresponding author. E-mail: zhaosm@njupt.edu.cn

© 2025 Chinese Physical Society and IOP Publishing Ltd. All rights, including for text and data mining, AI training, and similar technologies, are reserved.

the detecting rotational vibration using a beam-carrying OAM in a Sagnac interferometer.[22] Zhai *et al.* realized the angular acceleration detection based on the optical rotational Doppler effect of the OAM beam.[23] Emile *et al.* reported a naked-eye picometer resolution in Michelson interferometry using Laguerre–Gauss (LG) beams containing OAM.[24] Zhu *et al.* used the OAM of light to measure the dynamic micro-displacement and direction in real time, which demonstrated that the proposed sensor achieved high precision,[25] measured dynamic micro displacement, instantaneous velocity and the direction of motion simultaneously,[26] and used interference petals for dynamic micro-vibration measurement.[27] At present, it is possible to use OAM interferometry to measure the displacement of an object's movement, the direction of the movement, and also the tiny moving speed.

Based on the above OAM petal interferometry measurement work, in this paper, we propose a method to measure the object's flatness by generating a petal-like pattern with two OAM states with opposite topological charges. We obtain the relationship between the rotation angle of the petal-like patterns and the flatness of the detected object at first, then we validate the proposed measurement scheme by experiment.

The proposed flatness measurement method has some advantages and limitations. Firstly, and most importantly, it has a high precision. The experimental results show that for the 1.02 mm glass sample, the mean deviation of the flatness is 1.357×10^{-8} and the variance is 0.2142×10^{-16}. For 0.50 mm glass sample, the mean deviation of the flatness is 1.931×10^{-8} and the variance is 2.405×10^{-16}. Secondly, it has a wide applicability due to no contact. One can redesign the experimental setup to avoid contacting the object, like the setups in our works.[25,26] Here, the setup is only adopted for convenience. Normally, there are three different types of optical interferometry, such as monochromatic laser interferometry, low-coherence interferometry, and spectral interferometry.[7] Compared to the existing optical interferometry methods, the proposed method can avoid the 2π ambiguity problem in the monochromatic laser interferometry method, has a faster measurement speed than that of the low-coherence interferometry method, and does not need the wide wavelength range and high wavelength resolution of the spectrometer in the spectral interferometry method. Of course, there are some limitations to the proposed method. For example, the method is easily disturbed by the environmental disturbance due to the interferometric system structure, and has a smaller non-ambiguity range in comparison with the low-coherence interferometry method.

2. Theory

The schematic diagram of the proposed flatness measurement scheme is illustrated in Fig. 1. A Gaussian beam from the laser is turned into an OAM beam when it is passed through a spiral phase plate (SPP), or is reflected from a light spatial modulator (SLM) which is carrying a phase distribution of an LG mode. For an LG-OAM beam, ℓ is the azimuthal index giving an OAM of $\ell\hbar$ per photon, and p is the number of radial nodes in the intensity distribution. Under cylindrical coordinates, the electric field amplitude of an LG-OAM beam propagating along the z-axis direction can be expressed as[13,28]

$$\begin{aligned} &LG_p^{\ell}(r,\theta,z) \\ &= \sqrt{\frac{2p!}{\pi(p+|\ell|)!}}\frac{1}{w(z)}\left[\frac{r\sqrt{2}}{w(z)}\right]^{|\ell|} \\ &\times \exp\left[\frac{-r^2}{w^2(z)}\right] L_p^{|\ell|}\left(\frac{2r^2}{w^2(z)}\right)\exp[\mathrm{i}\ell\theta]\exp\left[\frac{\mathrm{i}k_0r^2z}{2(z^2+z_{\mathrm{R}}^2)}\right] \\ &\times \exp\left[-\mathrm{i}(2p+|\ell|+1)\tan^{-1}\left(\frac{z}{z_{\mathrm{R}}}\right)\right], \end{aligned} \tag{1}$$

where the $1/\mathrm{e}$ radius of the Gaussian term is given by $w(z) = w(0)\left[\left(z^2+z_{\mathrm{R}}^2\right)/z_{\mathrm{R}}^2\right]^{1/2}$ with $w(0)$ being the beam waist, z_{R} is the Rayleigh range, and $(2p+|\ell|+1)\tan^{-1}(z/z_{\mathrm{R}})$ is the Gouy phase. $L_p^{|\ell|}(x)$ is an associated Laguerre polynomial.[13] When $p=0$, Eq. (1) can be rewritten in a simpler form as[25]

$$E_\ell(r,\theta,z) = A(r,z)\exp(\mathrm{i}\ell\theta), \tag{2}$$

where $A(r,z)$ represents the amplitude information, and θ is the azimuthal index.

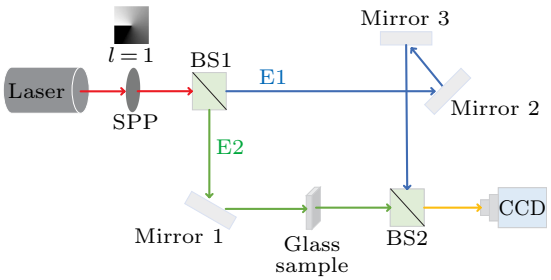


Fig. 1. The schematic diagram of the proposed measurement method based on OAM interference.

Then, the OAM beam is divided into a reference beam (E_1) and a measurement beam (E_2) through a beam splitter (BS1). After the reflections of mirror 2, mirror 3 and BS2, the reference beam is expressed as

$$E_1(r,\theta,z) = A_1(r,z)\exp(-\mathrm{i}\ell\theta). \tag{3}$$

On the other hand, after it is first reflected by mirror 1 and then passes through an object (for example, a glass sample), the measurement beam can be described as

$$E_2(r,\theta,z) = A_2(r,z)\exp(\mathrm{i}\ell\theta)\exp(\mathrm{i}knd), \tag{4}$$

where d is the thickness of the sample (such as glass), n is the refractive index of the glass sample, $k=2\pi/\lambda$ is the wave number and λ is the wavelength of the beam. Finally, the petal-like patterns are generated by the interference at BS2,

and can be recorded by a charge-coupled device (CCD), that is,

$$\begin{aligned} I &= |E_1(r,\theta,z)+E_2(r,\theta,z)|^2 \\ &= (E_1(r,\theta,z)+E_2(r,\theta,z))(E_1(r,\theta,z)+E_2(r,\theta,z))^* \\ &= |A_1(r,z)|^2+|A_2(r,z)|^2 \\ &\quad +2|A_1(r,z)||A_2(r,z)|\cos(2\ell\theta+knd), \end{aligned} \tag{5}$$

where the number of interfered petals is 2ℓ. The petal-like pattern should be rotated at the instant the glass sample is in or out. In order to measure the petals' rotation angle precisely, the maximum value of intensity is selected as the feature point, that is, the brightest position at each petal when $2\ell\theta+knd=2m\pi$ $(m=0,1,2,3,\ldots)$. Hence, the angle of each feature point can be described as

$$\theta=-\frac{\pi nd}{\lambda\ell}+\frac{m\pi}{\ell}. \tag{6}$$

Furthermore, for the same object (the same glass sample), the relationship between the flatness of the object (Δd) and the angle of the petal's rotation ($\Delta\theta$) can be described as

$$\Delta\theta=-\frac{\pi n\Delta d}{\lambda\ell}. \tag{7}$$

It is shown that the $\Delta\theta$ increases with the flatness of the glass sample Δd. Therefore, one can obtain the relationship between the flatness of the glass sample Δd and the petal rotation angle $\Delta\theta$, when ℓ and n are fixed,

$$\Delta d=-\frac{\lambda\ell}{n\pi}\Delta\theta. \tag{8}$$

In addition, we can obtain the flatness direction according to the rotation direction. If the petals are in the clockwise rotation, the flatness is concave. While it is convex, the petals are rotated anticlockwise. By measuring the rotation angle and direction of the petal-like pattern, the flatness of the glass sample can be measured and analyzed.

Here, we also present a detection method for detecting the rotation angle and the direction of the petal-like patterns by the intensity values on the sampling point. The details are described in Fig. 2 with the following steps.

(1) Obtaining a symmetrical petal pattern and taking the petal pattern picture at the center of the camera, then fitting out the center point of the pattern image, recorded as (x_0,y_0). Arbitrarily selecting a radius (r) (with which a circle can cross the symmetrical petals with the selected center point (x_0,y_0)), then drawing the sampled circle (the green circle) with the parameters (x_0,y_0), r. The center point (x_0,y_0), the radius r and the sampled circle (the green circle) can then be obtained in the original petal-like pattern.

(2) Archiving the intensity distribution values at the sampled point on the original petal-like pattern with the sample points. The sampled circle is sampled with the angle ($\theta=\frac{2\pi}{M}m$), where $m=1,\ldots,M$ and M are sample numbers. So each sampled point (x_m,y_m) at Fig. 2(a) can be depicted as

$$\begin{cases} x_m=x_0+r\cdot\cos\left(\dfrac{2\pi}{M}m\right), \\ y_m=y_0+r\cdot\sin\left(\dfrac{2\pi}{M}m\right). \end{cases} \tag{9}$$

With the intensity distribution, the maximum intensity point (A_1 at Fig. 2(b)) and its corresponding coordinate values can be obtained (for instance, $M_1=751.752$).

(3) Taking the rotated petal pattern picture when the glass sample is added to the optical path, drawing a sampled circle (the green circle) with the parameters (x_0,y_0), r as shown in Fig. 2(c). It is noted that the parameters (x_0,y_0), r are the same as those at step 1.

(4) Archiving the maximum intensity point (A_2 at Fig. 2(d)) and its corresponding coordinate values (for example, $M_2=17.107$) for the rotated petal-like patterns. Then, the rotation angle is computed as

$$\Delta\theta=\frac{2\pi}{M}(M_1-M_2). \tag{10}$$

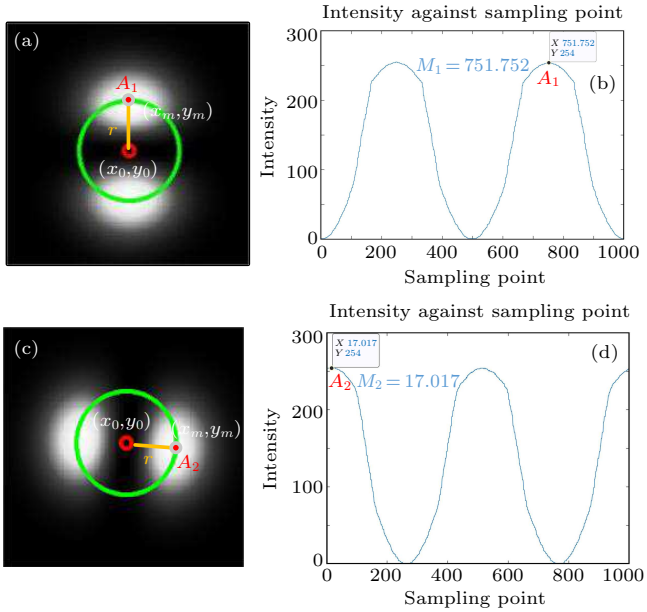


Fig. 2. (a) Obtaining the center point, the radius and the sampled circle for the petal-like pattern without object (named original petal-like pattern), (b) archiving the intensity distribution at the sampling point on the original petal-like pattern A_1, (c) drawing the sampled circle for the petal-like pattern with the object (named the rotated petal-like pattern) with the obtained center point, radius, (d) archiving the intensity distribution at the sampling point on the rotated petal-like pattern A_2.

3. Experimental result

In this section, we discuss the feasibility of the proposed method by experiment. Figure 3 is the experimental setup for the proposed scheme. The Gaussian beam with wavelength 632.8 nm is generated by a diode-pumped solid-state laser (MGL-III-632-100 mW). A spatial light modulator (SLM, Holoeye PLUTO-2-VIS, 1920 × 1080 pixels, pixel

pitch 8.0 μm) is used to generate an OAM beam. After the first beam splitter, the beam is divided into a reference beam and a measurement beam. The measurement beam passes through an optical uniformity glass sample, which has a refractive index of 1.47 and a good light homogeneity, and the size is 25 mm×25 mm. Finally, the petal patterns are generated at another beam splitter, and captured by a CCD (Thorlabs, Model BC106N-VIS/M).

The petal-like interference patterns at each detection point are recorded by CCD. Nine detection points labeled as A to I in Fig. 3 are used to be detected so that the measurement beam can pass through different areas, and 5 times for each detection point are adopted to archive the average value. Nine detection points are selected because the flatness of the glass sample can be obtained due to its unflatness. Here, the selection of the nine points (nine locations on the sample) is arbitrary. In order to make the experimental measurement be more convenient, we choose randomly point (A) at first, then we move 6 mm horizontally to get point B, since the scale in the experimental platform is 1 mm, it is easy to locate point B, then locate point C in the same way. Similarly, we can locate point D from point A by moving vertically 6 mm. With horizontal and vertical moving (6 mm), all nine measurement points can be achieved with the same strategy.

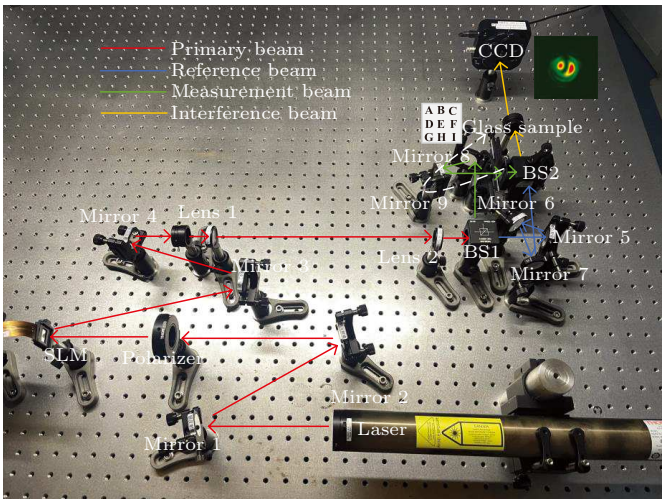


Fig. 3. The experimental setup for the proposed method with OAM interference. BS: beam splitter, SLM: spatial light modulator.

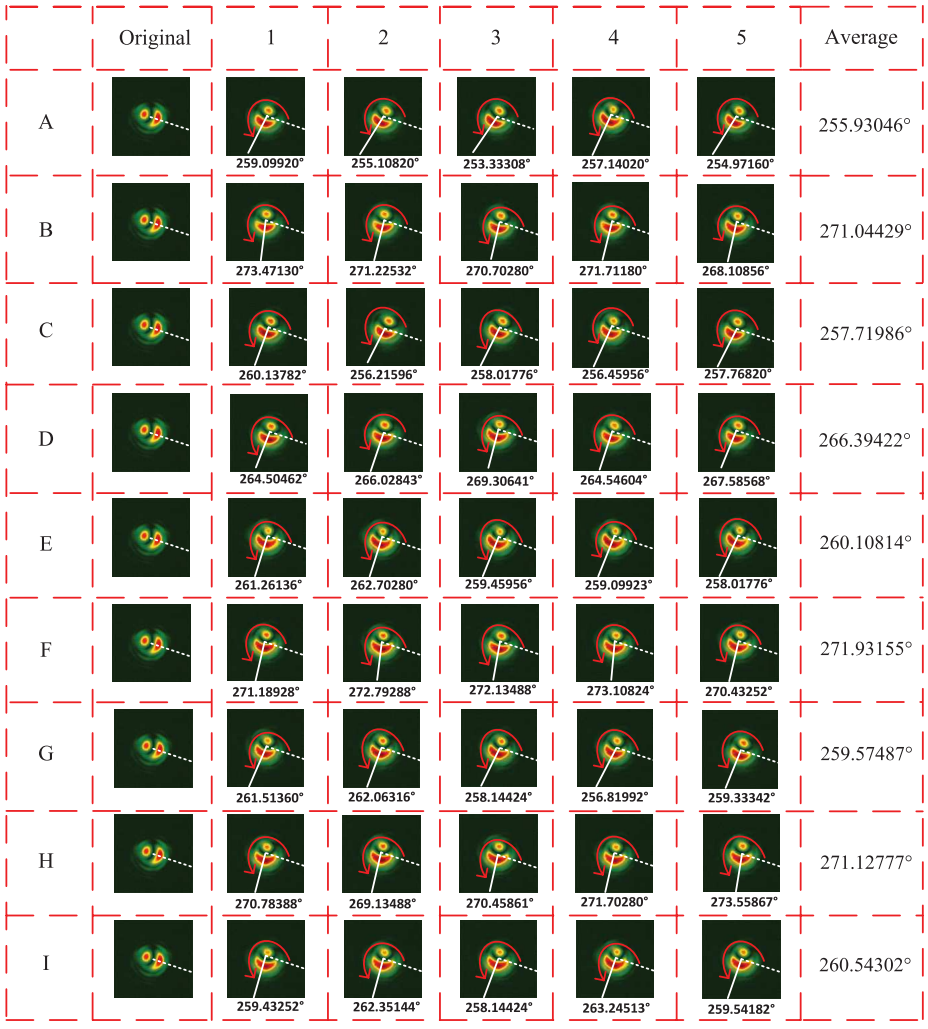


Fig. 4. The interference petal-like patterns for nine points, together with the rotated angle degrees. These are performed five times for each point from A to I. The thickness of the glass sample is 1.02 mm.

Figure 4 shows the interfered petal-like patterns at A to I (9 points) for a glass sample (1.02 mm), together with their evaluated rotation angles. The topological charge of the used LG beam is 1. These are performed five times for each detection point from A to I. We calculate the angle of petal rotation by using the method mentioned above. For example, for point A in Fig. 4, according to the method described in Fig. 2, the maximum intensity points $M_1 = 769.77$ and $M_2 = 50.05$ are measured, where $M = 1000$, then the rotation angle (259.09920°) can be calculated by Eq. (10). The results show that with the proposed method and the presented detection scheme, one can obtain the rotation angles when the glass sample is in/out. For the different detection points, the rotated angles are different. In addition, the rotated angle at one point has small fluctuations for different time measurements due to the environmental disturbance.

Then we list all the thicknesses calculated from the rotated angles and the corresponding flatness in Table 1, where two glass samples are used: one thickness is 0.50 mm, the other is 1.02 mm. The thickness corresponding to each point is the result of averaging the five measurements.

Here, the flatness deviation (D) and the variance (V) are used to express the precision. Both the flatness deviation and the variance are defined as

$$\begin{aligned} D &= \left|T_{\text{mearsured}} - T_{\text{sample}}\right|, \\ \overline{D} &= \frac{\sum_{i=1}^{n} D(i)}{n}, \\ V &= \frac{\sum_{i=1}^{n} (D(i) - \overline{D})^2}{n}, \end{aligned} \tag{11}$$

where $T_{\text{mearsured}}$ is the calculated thickness by the mean measured rotation angle, T_{sample} is the real thickness of the sample provided by the manufactory, $D(i), i \in A, \ldots, I$ are the calculated flatness deviations for each measured point, and n is the measurement point number, here it is 9. The smaller flatness deviation variance indicates a good flatness, while a larger deviation variance value indicates a bad one. We measure the flatness of different positions and obtain the corresponding flatness deviations. For the 1.02 mm glass sample, the mean deviation of the flatness is 1.357×10^{-8} and the variance is 0.242×10^{-16}. For the 0.50 mm glass sample, after the measurements and the thickness calculations, the mean deviation is 1.931×10^{-8} and its variance is 2.405×10^{-16}. The smaller value of the deviation variance indicates the smoother surfaces the glass sample (1.02 glass sample) has.

Table 1. The mean rotation angle, calculated thickness and their flatness deviation for the two glass samples.

		Mean rotation angle (°)	Calculated thickness (mm)	Flatness deviation D ($\times 10^{-8}$)
A	1.02 mm	255.93046	1.0199797	2.03
	0.50 mm	267.74784	0.4999927	0.73
B	1.02 mm	271.04429	1.0200158	1.58
	0.50 mm	278.32441	0.5000181	1.81
C	1.02 mm	257.71986	1.0199839	1.61
	0.50 mm	252.16227	0.4999554	4.46
D	1.02 mm	266.39422	1.0200047	0.47
	0.50 mm	271.40292	0.5000015	0.15
E	1.02 mm	260.10814	1.0199897	1.03
	0.50 mm	251.74786	0.4999545	4.55
F	1.02 mm	271.93155	1.0200179	1.79
	0.50 mm	263.18928	0.4999818	1.82
G	1.02 mm	259.57487	1.0199884	1.16
	0.50 mm	275.17126	0.5000105	1.05
H	1.02 mm	271.12777	1.0200162	1.62
	0.50 mm	264.60673	0.4999852	1.48
I	1.02 mm	260.54302	1.0199907	0.93
	0.50 mm	276.36946	0.5000133	1.33

According to the obtained data in Fig. 4 and Table 1, we also can determine the concave or convex conditions of the glass sample. For instance, in Fig. 4, the petal-like pattern at position B is rotated counterclockwise relative to that of position A. Applying the directional judgment method outlined in the theoretical section, we can obtain that position B is more convex than that of position A.

This can also be verified by the data in Table 1. For the 0.50 mm glass sample, the petal-like pattern is rotated counterclockwise. The result shows that the rotated angle at position D is 271.40292°, which is greater than that of position A (267.74784°), therefore, the petal-like pattern at position D is relatively rotated counterclockwise in comparison with position A, so we can obtain that position D is more convex than that of position A. At the same time, the rotation angle at position E (251.74786°) is rotated clockwise relative to that at position F (263.18928°), hence, point E is concave to that of position F. It is shown that the concavity or convexity of the glass sample can be obtained by the rotation direction of the petal-like pattern. All the results show that the proposed

method can measure the flatness with a smaller deviation variance with convexity.

4. Discussion

In this section, we present some discussions on the proposed method.

Firstly, we discuss the impact of environmental disturbance on the proposed method. We perform an experiment, and continuously record the interference petals for 1 minute without the added object. Figure 5 demonstrates 6 frames for every 12 seconds when the air conditioner is turned on/off. The angle values of rotation are calculated and listed. According to the calculation, it is shown that the angle is affected by the environment, but the average rotation is much smaller (2.9192° when the air conditioner is turned on, and 0.1632° when the air conditioner is turned off), which is much smaller than those rotation angles caused by the roughness of the glass sample. As can be seen from Table 1, the rotation angle is about 15° when the detection point is moved from point A to point B for the glass sample with 1.02 mm. It hints that the roughness of the glass is the main factor on the rotated angle, and the impact of the environment can be reduced by multiple measurements. Furthermore, the main environmental disturbance may come from the vibrations caused by air conditioning noise.

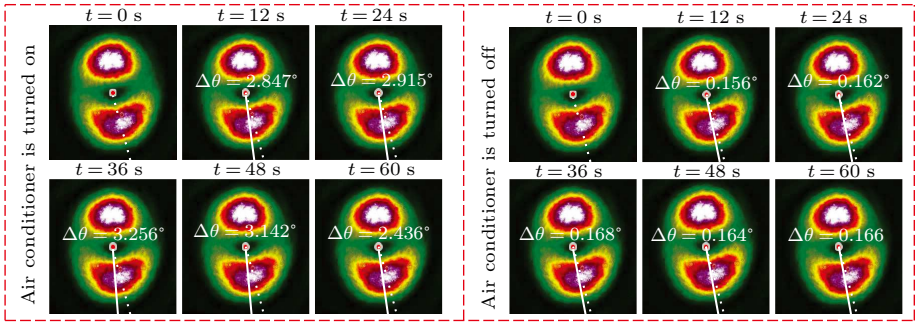


Fig. 5. The interference petal-like pattern recorded at every 12-second interval during 1 minute when the air conditioner is turned on/off.

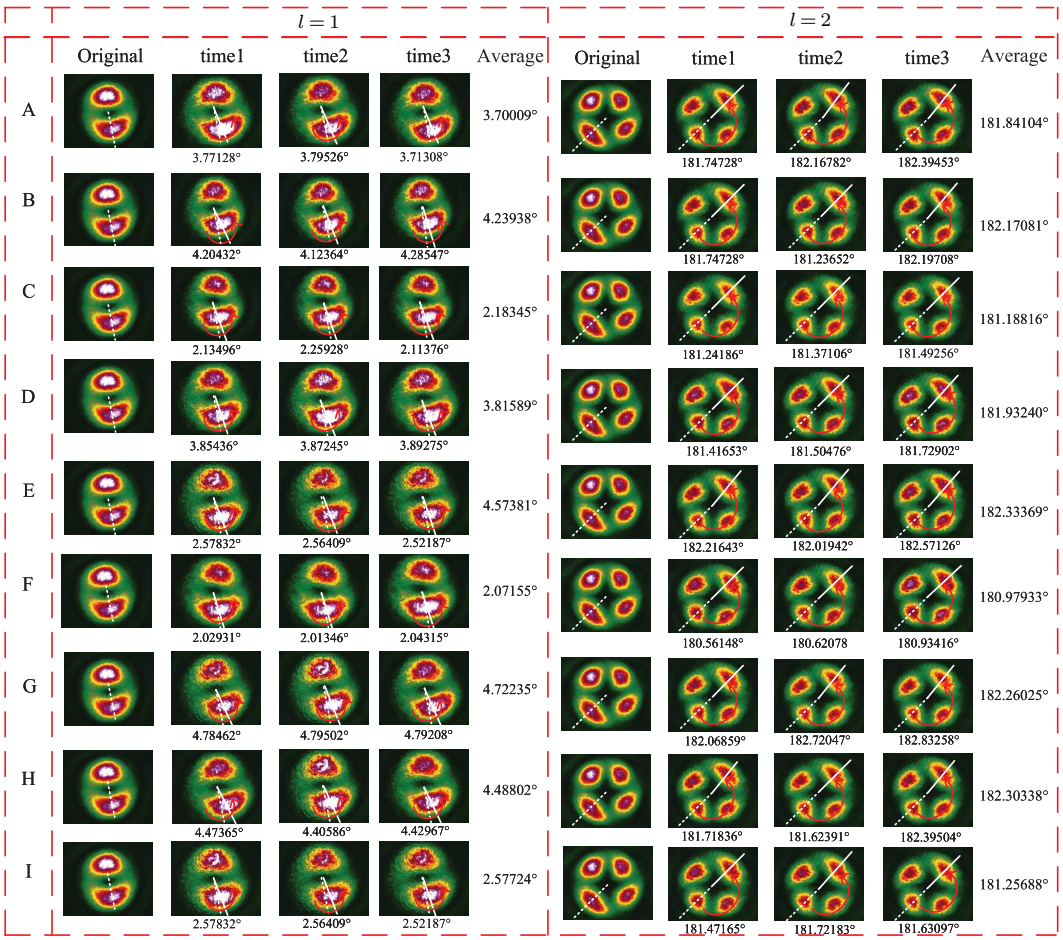


Fig. 6. The interference petal-like patterns for nine points, together with the rotated angle degrees. These are performed five times for each point from A to I. The thickness of the glass sample is 2.00 mm with $\ell = 1$ and $\ell = 2$, respectively.

Secondly, we discuss the impact of the used topological charge on the proposed method. We measure the flatness of a new glass sample with 2.00 mm, and record all the rotation angle's changes under $\ell = 1$ and $\ell = 2$, respectively when the air conditioner is turned off. Figure 6 shows the interference petal-like pattern of nine points (A–I) and their rotation angles under $\ell = 1$ and $\ell = 2$, respectively. Here, each measurement point is measured five times, and only three of them are demonstrated in the figure. The average value of the five times measurement results is adopted to calculate the flatness of the glass sample. The results show that for the 2.0 mm glass sample, the flatness measured by the proposed method has almost the same precision when the used topological charges are different. Compared with those results in Fig. 4, the fluctuations among the five measured results at the same point become smaller, which indicates that the impact of the environmental disturbance on the proposed method has been reduced by turning off the air conditioner.

Similarly, we list all the mean rotation angles in Fig. 6, calculated thicknesses and their flatness deviations in Table 2, when two different topological charges ($\ell = 1$ and $\ell = 2$) are adopted.

Table 2. The mean rotation angle, calculated thickness and their flatness deviations D with different topological charges.

		Mean rotation angle (°)	Calculated thickness (mm)	Flatness deviation D ($\times 10^{-8}$)
A	$\ell = 1$	3.70009	2.0000012	0.12
	$\ell = 2$	181.84104	2.0000012	0.12
B	$\ell = 1$	4.23938	2.0000025	0.25
	$\ell = 2$	182.17081	2.0000028	0.28
C	$\ell = 1$	2.18345	1.9999981	0.19
	$\ell = 2$	181.18816	1.9999981	0.19
D	$\ell = 1$	3.81589	2.0000015	0.15
	$\ell = 2$	181.93240	2.0000016	0.16
E	$\ell = 1$	4.57381	2.0000033	0.33
	$\ell = 2$	182.33369	2.0000035	0.35
F	$\ell = 1$	2.07155	1.9999973	0.27
	$\ell = 2$	180.97933	1.9999971	0.29
G	$\ell = 1$	4.72235	2.0000037	0.37
	$\ell = 2$	182.26025	2.0000032	0.32
H	$\ell = 1$	4.48802	2.0000031	0.31
	$\ell = 2$	182.30338	2.0000034	0.34
I	$\ell = 1$	2.57724	1.9999985	0.15
	$\ell = 2$	181.25688	1.9999984	0.16

For the 2.00 mm glass sample, the mean deviation of flatness is evaluated as 0.239×10^{-8} and its variance is 0.799×10^{-18} when $\ell = 1$. Similarly, for the same glass sample, the mean deviation of the flatness is 0.246×10^{-8} and the variance is 0.775×10^{-18} when $\ell = 2$. It is shown that for the same sample, the proposed measurement method has the same results when different topological charges are adopted. At the same time, compared to the results in Table 1, the flatness deviation values for the nine measurement points are decreased in Table 2, when the air conditioning is turned off. Simultaneously, the variance of the flatness deviation ($0.799\times10^{-18}, \ell = 1$) is greatly reduced in comparison with the variance evaluated in Table 1. It is shown that the environmental disturbance can be reduced by turning off the air conditioner. However, the difficulty in locating the maximum intensity points (M_1 and M_2 shown in Fig. 2) is increased when a larger topological charge is used, thus affecting the measurement result.

5. Conclusion

In the paper, we present a measurement method for the flatness of an object by using the petal-like patterns generated by the interference of two Laguerre–Gaussian beams carrying opposite. By calculating the petal rotated angle caused by the coaxial interference between the measured OAM beam and the reference OAM beam, the thickness information, then the flatness information can be evaluated. The concave and convex direction of the target surface is also determined by the petal-like pattern rotation direction. In order to reduce the influence of environmental disturbance during the experiment, multiple measurements are adopted at each detection point, and the average rotated angles are used for the flatness calculation. Three different thickness glass samples are used for the experiments, and their flatness deviations are 1.357×10^{-8} (1.02 mm glass sample), 1.931×10^{-8} (0.50 mm glass sample), 0.239×10^{-8} (2.00 mm glass sample, $\ell = 1$), and 0.246×10^{-8} (2.00 mm glass sample, $\ell = 2$), respectively. Correspondingly, their variance are 0.242×10^{-16}, 2.405×10^{-16}, 0.799×10^{-18} ($\ell = 1$), 0.775×10^{-18} ($\ell = 2$), respectively. The experimental results show that the proposed method can realize a high-precision flatness measurement. For the same glass sample with different topological charges, the measurement results are almost the same, and the flatness variance can be greatly reduced by suppressing the environmental disturbance.

Acknowledgements

Project supported by the National Natural Science Foundation of China (Grant No. 62375140) and the Open Research Fund of National Laboratory of Solid State Microstructures (Grant No. M36055).

References

[1] Zhang M, Liu Y, Sun C, *et al.* 2020 *Meas. Sci. Technol.* **31** 085006
[2] Xu C, Chen L, Chen S and Yin J 2009 *Appl. Opt.* **48** 2536
[3] Fu Y, Shang Y, Hu W, *et al.* 2021 *Acta Mech. Sin.* **37** 537
[4] Rusli and Amaratunga G A J 1995 *Appl. Opt.* **34** 7914
[5] Koirala P, Attygalle D, Aryal P, *et al.* 2014 *Thin Solid Films* **571** 442
[6] Yu Q, Zhang K, Cui C C, *et al.* 2018 *Appl. Opt.* **57** 9722
[7] Park J, Kim J A, Ahn H, *et al.* 2019 *Precis. Eng. Manuf.* **20** 463
[8] Allen L, Beijersbergen M W, Spreeuw R J C and Woerdman J P 1992 *Phys. Rev. A* **45** 8185
[9] Liu J, Zheng S, Chen S, *et al.* 2022 *Appl. Phys. Lett.* **120** 131103
[10] Wang X, Qian Y, Zhang J, *et al.* 2021 *Photon. Res.* **9** B81
[11] Sasaki S and Mcnulty I 2008 *Phys. Rev. Lett.* **100** 124801
[12] Wang J, Yang J Y, Fazal I M, *et al.* 2012 *Nat. Photonics* **6** 488
[13] Yao A M and Padgett M J 2011 *Adv. Opt. Photonics* **3** 161
[14] Lei T, Zhang M, Li Y R, *et al.* 2015 *Light Sci. Appl.* **4** e257
[15] Tang H, Xu W, and Wu G H 2016 *China. Commun.* **13** 153
[16] Wu J Z and Li Y J 2007 *Chin. Phys. B* **16** 1334
[17] Guo J, Zheng S, Zhou K and Feng G 2021 *Phys. Rev. Lett.* **119** 023504
[18] Yan Y, Li L, Xie G D, *et al.* 2016 *Sci. Rep.* **6** 33482
[19] Lavery M P J, Speirits F C, Barnett S M and Padgett M J 2013 *Science* **341** 537
[20] Guo J X, Ming S, Wu Y, Chen L Q and Zhang W P 2021 *Opt. Express* **29** 208
[21] Zhai Y W, Fu S Y, Zhang J Q, *et al.* 2020 *Appl. Phys. Express* **13** 022012
[22] Xiao S X, Zhang L D, Wei D, Liu F, Zhang Y and Xiao M 2018 *Opt. Express* **26** 1997
[23] Zhai Y W, Fu S Y, Yin C, Zhou H and Gao C Q 2019 *Opt. Express* **27** 15518
[24] Emile O and Emile J 2017 *Opt. Express* **42** 354
[25] Zhu J L, Wang L, Ji J Y and Zhao S M 2022 *Appl. Phys. Lett.* **120** 251104
[26] Zhu J L, Han F F, Wang L and Zhao S M 2024 *J. Lightwave Technol.* **42** 1689
[27] Zhu J L, Zou F C, Wang L and Zhao S M 2024 *Photonics* **11** 27
[28] Allen L , Padgett M and Babiker M 1999 *Prog. Opt.* **39** 291